

Optimal landing site selection based on safety index during planetary descent



Pingyuan Cui^{a,b,c}, Dantong Ge^{a,b,c}, Ai Gao^{a,b,c,*}

^a School of Aerospace Engineering, Beijing Institute of Technology, Beijing 100081, China

^b Key Laboratory of Autonomous Navigation and Control for Deep Space Exploration, Ministry of Industry and Information Technology, Beijing 100081, China

^c Key Laboratory of Dynamics and Control of Flight Vehicle, Ministry of Education, Beijing 100081, China

ARTICLE INFO

Keywords:

Safe landing
Landing site selection
Safety index

ABSTRACT

Landing safety is the prior concern in planetary exploration missions. With the development of precise landing technology, future missions require vehicles to land on places of great scientific interest which are usually surrounded by rocks and craters. In order to perform a safe landing, the vehicle should be capable of detecting hazards, estimating its fuel consumption as well as touchdown performance, and locating a safe spot to land. The landing site selection process can be treated as an optimization problem which, however, cannot be efficiently solved through traditional optimization methods due to its complexity. Hence, the paper proposes a synthetic landing area assessment criterion, safety index, as a solution of the problem, which selects the best landing site by assessing terrain safety, fuel consumption and touchdown performance during descent. The computation effort is cut down after reducing the selection scope and the optimal landing site is found through a quick one-dimensional search. A typical example based on the Mars Science Laboratory mission is simulated to demonstrate the capability of the method. It is proved that the proposed strategy manages to pick out a safe landing site for the mission effectively. The safety index can be applied in various planetary descent phases and provides reference for future mission designs.

1. Introduction

Planetary landing site selection is a trade-off between safety and science interest, and the primary goal to achieve in the descent phase is to ensure the vehicle lands on the surface safely [1]. Based on the remote sensing data acquired by the orbiters, the areas suitable for landing are investigated and compared. Selecting criteria of an ideal landing site are similar in spite of different exploration objects. These criteria mainly include science return, illumination, latitude, elevation, surface roughness, slope, etc. [2–4]. Landing sites which offer the prospect of analyzing a variety of rocks and soil tend to be more appealing as they provide answers to questions like differentiation of the crust, weathering development, nature of the early environment and its evolution [5]. These areas of great scientific interest, however, are usually full of hazards [6], which threatens landing safety and sets high requirements on landing accuracy [7]. As the lander approaches its destination, a better knowledge of the surface is obtained [8]. The pre-determined landing site might turn out to be not acceptable according to the engineering constraints or trajectory analyses [4,9]. Besides, it is possible that the original landing site is surrounded by

small but fatal hazards, which cannot be detected until the vehicle is close enough to the surface [10]. Similar situations occurred during Hayabusa's first rehearsal descent when one of the landing sites 'Woomera Desert' was found not suitable for sampling since the area was covered with much more boulders than anticipated [11]. In addition, during descent, the vehicle's position may be largely deviated from the nominal trajectory due to environmental uncertainties and accumulated navigation errors [12] and the pre-designed landing site may be out of sight. To solve these problems and improve landing safety, further analysis of the landing area is required so that a proper place can be picked out for landing and the descent trajectory can be adjusted accordingly [13].

In the past years, safe landing is mainly achieved by hazard detection and avoidance [14,15]. Terrain condition determined by rocks, craters and slopes is evaluated and a flat area free of hazards is selected as the final landing site [16]. To accomplish a safe landing, there are some other factors that should also be taken into account. In Serrano's work, terrain safety derived from on-board sensors, landing footprint based on spacecraft descent dynamics, and regions of science interest are incorporated to locate the best landing site using prob-

* Corresponding author at: Mail box 22, School of Aerospace Engineering, Beijing Institute of Technology, Beijing, China.
E-mail addresses: cui.py@bit.edu.cn (P. Cui), gedt@bit.edu.cn (D. Ge), gaoai@bit.edu.cn (A. Gao).

abilistic reasoning which is capable of making decisions based on imprecise and uncertain information [17]. Later on, Cohanin presents a weighted cost function of distance to nearest hazards, distance to nearest points of interest, and ΔV contours [10]. The function is a two-dimensional cost map and by using a greedy algorithm, landing aim points that are safe, close to areas of interest, and minimize diverts are chosen. These works offer effective solutions for landing site selection by adding engineering constraints and scientific concerns into the process. In the descent phase, for safety concerns, some mission-determined factors like the touchdown performance may also affect landing safety, which have not been considered in the assessment work before. Besides, the landing site selection process is supposed to be conducted online. In this way, both the computation efficiency and memory capacity are limited, which challenges the availability of the selection method.

In this paper, after analyzing the influences of terrain safety, fuel consumption and touchdown performance on landing safety, the landing site selection process is converted into an optimization problem for the first time. The safety index is then proposed as an effective solution. The content of the index corresponds with the factors shown in the optimization problem and the specific normalization method adopted by each factor is determined by its form in the problem. The optimal landing site is found efficiently using a one-dimensional search. By implementing the safety index-based landing site selection method, the vehicle manages to avoid the hazards and land on the surface with limited propellant and better landing performance.

The paper is organized as follows. In Section 2, both objective and mission-determined factors associated with landing safety in the descent phase are analyzed and the mathematical model is built. The optimization form of the landing site selection problem is given and the difficulty in solving is stated. The safety index is then proposed in Section 3 as a transformation of the problem and selects the optimal landing site with a reduced amount of computation after narrowing down the selection scope. A MSL-based simulation is conducted in Section 4 using the safety index as an illustration of how it functions in planetary landing missions, followed by the conclusion in Section 5.

2. Problem formulation

In order to increase the success probability of the landing mission, the possible landing area needs to be carefully assessed before a specific location is designated for the vehicle to land on. As past works [4,11,18] suggest, landing site selection is more than hazard detection and avoidance. Aspects that may affect landing safety like fuel consumption and touchdown performance should also be taken into account. Note that in practical missions, the reason that causes landing failure can be very sophisticated. In this paper, we only discuss the impact of terrain safety, fuel consumption and touchdown performance on landing site selection.

2.1. Terrain safety

As the vehicle approaches the surface, specific terrain information of high resolution is obtained [8]. Small hazards including rocks, craters and slopes can then be observed and detected. When selecting a suitable place to land, areas with steep slope and rocky surface should be avoided as they may threaten landing safety and impact subsequent science operations. Two primary terrain characteristics are chosen to be considered in the terrain safety analysis, that is, local slope and surface roughness [19], as illustrated in Fig. 1.

During descent, the Digital Elevation Model (DEM) is obtained from the operational sensors. The local fitting plane is estimated by [20]

$$aX + bY + cZ = 1 \tag{1}$$

a, b, c are the fitting parameters as well as the three components of the normal vector \mathbf{n} , which can be solved using the standard least-squares plane-fitting algorithm

$$\mathbf{n} = [a \ b \ c]^T = (\mathbf{G}^T \mathbf{G})^{-1} \mathbf{G}^T \mathbf{h} \tag{2}$$

$$\mathbf{G} = \begin{bmatrix} x_1 & y_1 & z_1 \\ x_2 & y_2 & z_2 \\ \vdots & \vdots & \vdots \\ x_N & y_N & z_N \end{bmatrix} \tag{3}$$

$$\mathbf{h} = [1 \ 1 \ \dots \ 1]^T \tag{4}$$

$\mathbf{G}\mathbf{h}$

The local slope is obtained by computing the angle between the normal vector of the plane \mathbf{n} and the local gravity direction $\mathbf{b} = [0 \ 0 \ 1]^T$, and is expressed by

$$\varphi = \cos^{-1} \left(\frac{|\mathbf{n}^T \cdot \mathbf{b}|}{\|\mathbf{n}\| \cdot \|\mathbf{b}\|} \right) = \cos^{-1} \left(\frac{|c|}{\sqrt{a^2 + b^2 + c^2}} \right) \tag{5}$$

The fitting error between the estimated plane and the DEM data is measured as the surface roughness [19]

$$d_l = \frac{|ax_l + by_l + cz_l - 1|}{\sqrt{a^2 + b^2 + c^2}}, \quad l = 1, 2, \dots, N \tag{6}$$

In this paper, the terrain within the landing area is considered safe if it satisfies both the slope and the roughness constraints

$$\varphi \leq \varphi_{\text{safe}} \tag{7}$$

$$d \leq d_{\text{safe}} \tag{8}$$

So far, the hazards in view are recognized. To pick out a suitable place to land, more works need to be done. As the main component of safety concerns, terrain safety is assessed from the following two aspects:

- a. The size of the hazards at the landing site must be within the tolerance of the vehicle shown in Eq. (7) and (8);
- b. The landing area should be large enough to tolerate the landing dispersion of the vehicle.

Both aspects should be met at the same time and this means not only the landing site, but also its vicinity should be hazard-free considering a certain landing dispersion. Thus, the safe radius R , defined as the distance between the pixel and its nearest hazards, is introduced into the assessment process. According to the hazard detection result, the computer onboard generates a grid map and divides the grid into safe pixels (marked as 1) and hazardous pixels (marked as 0) considering the tolerance of the vehicle. An ergodic search algorithm [13] is then applied to the binary map to calculate the safe radius R of every pixel. The larger the safe radius is, the further the threatening hazards are from the pixel. According to the definition, the safe radius values of the safe pixels are positive and the unsafe ones are zero.

$$\begin{cases} R_{ij} > 0, & (x_i, y_j) \in \text{SAFE} \\ R_{ij} = 0, & (x_i, y_j) \in \text{UNSAFE} \end{cases} \tag{9}$$

A simulated terrain model in Fig. 2 is built to verify the effectiveness of the algorithm. Fig. 3 illustrates the binary result of hazard detection (safe=1, hazardous=0) and the corresponding safe radius computation result is shown in Fig. 4.

2.2. Fuel consumption

Fuel consumption, on the concern of safety, does not necessarily need to be minimized as long as it's enough to send the vehicle to the landing site. However, if the task requires the vehicle to save some fuel

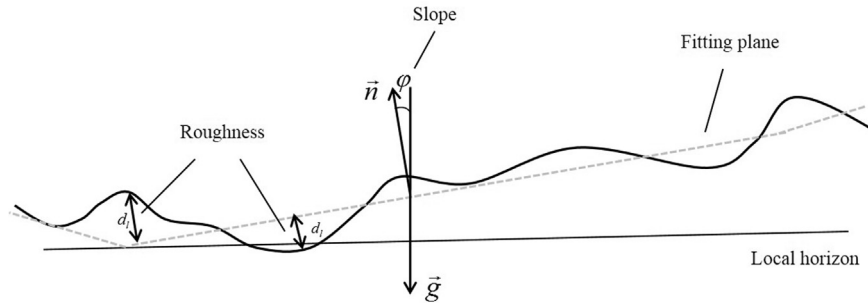


Fig. 1. Definition of terrain hazards.

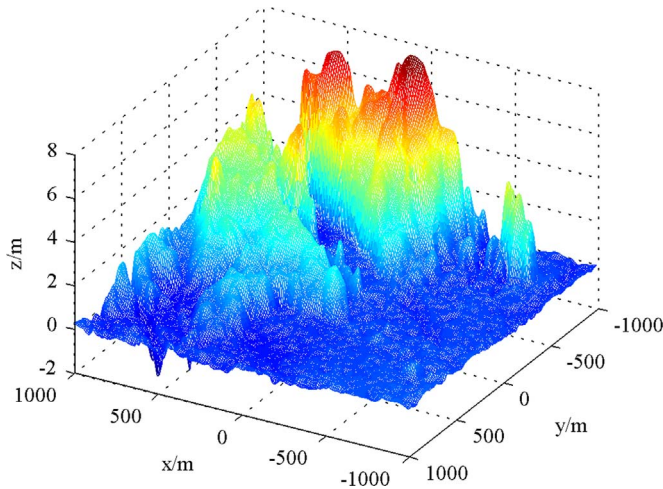


Fig. 2. The simulated terrain model.

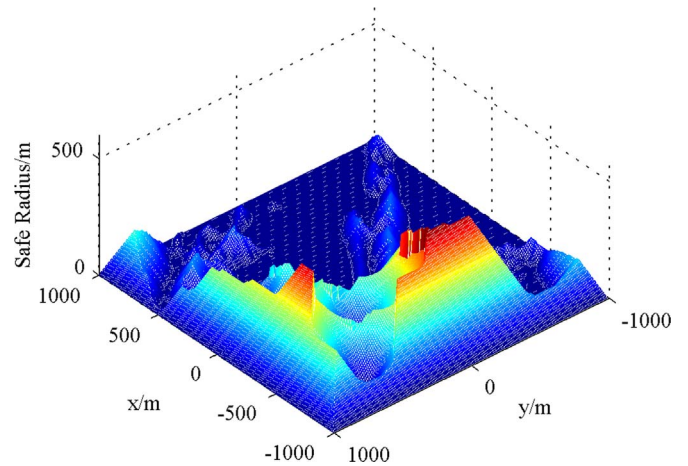


Fig. 4. The safe radius computation result.

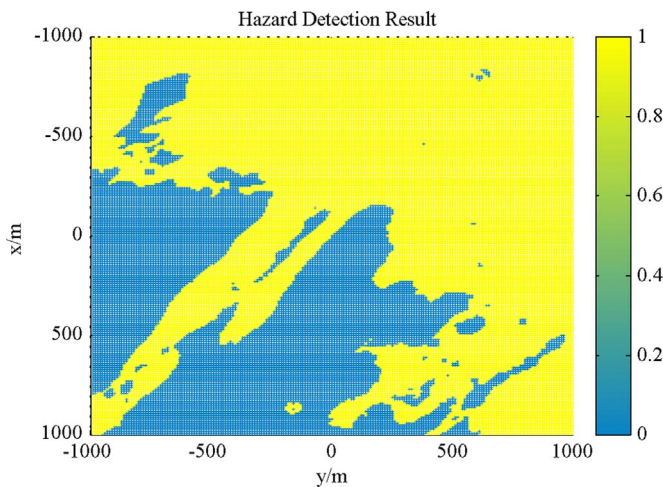


Fig. 3. The hazard detection result (safe=1, unsafe=0).

$$\begin{aligned}
 PMF_{ij} &= \left(\frac{\int_{t_0}^{t_f} \dot{m} dt}{m_0} \right)_{ij} = \left(\frac{m_0 - m_n}{m_0} \right)_{ij} = \left(1 - \frac{m_0 e^{-\frac{\sum_{k=1}^n \|a_k\| \Delta t}{I_{sp} g_e}}}{m_0} \right)_{ij} \\
 &= \left(1 - e^{-\frac{\sum_{k=1}^n \|a_k\| \Delta t}{I_{sp} g_e}} \right)_{ij}
 \end{aligned} \tag{10}$$

where the subscript ij refers to the value of the variable at (x_i, y_j) , m_0 is the initial mass of the vehicle, \dot{m} is the mass flow rate, a_k is the discrete acceleration in $[t_k, t_k + \Delta t]$, I_{sp} is the specific impulse of thrusters, and g_e is the gravitational acceleration on Earth. The value of PMF depends on both the vehicle's current state and the landing site location. Given a fixed initial state, it is shown in Fig. 5 that the PMF value varies at different landing points using the polynomial guidance law [22]. As can be seen, the further the point is from the center, the larger the PMF gets. This is mainly because in the simulation, the vehicle's initial

for possible emergency maneuvers, the fuel consumption during descent is the smaller the better. Besides, a landing site is viable only if the vehicle can reach it with a given amount of fuel [1]. The fuel consumption constraint can be included into the landing site selection process by either searching for the location that minimizes the index or constraining the landing area under assessment within the reachable region of the vehicle. Here the former fashion is used.

The Propellant Mass Fraction (PMF) is a useful metric for fuel consumption [12] and is chosen as the fuel consumption function. It is defined as the proportion of the propellant mass and the total wet mass of the vehicle and can be calculated by [21]

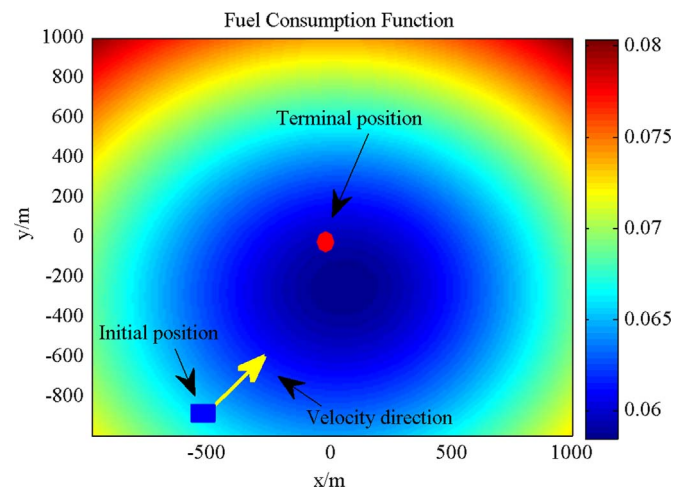


Fig. 5. The fuel consumption function map.

position is above the area at bottom left and its velocity direction points towards nearly the center of the map, which means the trajectory is straighter if the landing site is near the center and highly curved if it's at the edge of the map. Larger PMF value indicates more fuel consumption and it is likely to go beyond the maneuverability of the vehicle. Hence, areas that have smaller PMF values should be considered prior in landing site selection.

2.3. Touchdown performance

Besides the objective factors mentioned above, some mission-determined factors like the touchdown performance of the vehicle may also affect landing safety. In the descent phase, the main goal is to divert the vehicle to the designated landing site with minimal landing error and velocity. Meanwhile, the attitude control system is required to adjust the attitude of the vehicle to change the thrust direction during descent and vertically land on the surface. In the MSL mission, after heatshield separation, the performance of the vehicle is mainly based on the interaction with the ground and the EDL system is proved to be sensitive to the maximum terrain relief [23]. When selecting a proper landing site, high elevation or steep slopes that may lead to large impact velocity and inclined landing attitude should be kept away from the vehicle. Besides, the touchdown performance is also influenced by the external disturbance and internal error occurred during descent. Given the same initial states, the nominal state variations and the curvature of the flight path are different from each other when the location of the landing target changes. Thus, the impact of, for instance, the same wind disturbance or execution error on the touchdown performance varies.

Complete landing system characteristics can be revealed via valid numerical simulation but only the system responses relevant with the touchdown performance and landing safety are of interest in the landing site selection process. In the Rosetta mission, for example, the three main influencing touchdown condition parameters are the velocity magnitude, the flight path angle, and the attitude angle [24]. The three parameters cover the information of the landing velocity magnitude and direction, as well as the terminal attitude excursion of the lander body with regard to the local normal, and thus are chosen to evaluate the touchdown performance in this paper. The definitions of the parameters are given by

$$\begin{cases} \|v_f\|_{ij} = (\sqrt{v_{fx}^2 + v_{fy}^2 + v_{fz}^2})_{ij} \\ \gamma_{ij} = \cos^{-1}\left(\frac{|v_f^T \cdot g|}{\|v_f\| \cdot \|g\|}\right)_{ij} = \cos^{-1}\left(\frac{lgv_{fz}}{g\sqrt{v_{fx}^2 + v_{fy}^2 + v_{fz}^2}}\right)_{ij} \\ \alpha_{ij} = \cos^{-1}\left(\frac{|Z_b^T \cdot n|}{\|n\|}\right)_{ij} = \cos^{-1}\left(\frac{a_f^T \cdot n}{\|a_f\| \cdot \|n\|}\right)_{ij} = \cos^{-1}\left(\frac{laaf_x + ba_fy + ca_fz}{\sqrt{a_x^2 + a_y^2 + a_z^2} \sqrt{a^2 + b^2 + c^2}}\right)_{ij} \end{cases} \quad (11)$$

where v_f is the landing velocity, a_f is the landing acceleration, Z_b is the symmetry axis of the vehicle, g is the local gravity and $n = [a \ b \ c]^T$ is the local normal direction. Among the three parameters, the landing velocity magnitude $\|v_f\|$ is the 2-norm of the landing velocity v_f , the flight path angle γ_{ij} is obtained by calculating the angle between the landing velocity and the local gravity, and the landing attitude angle α_{ij} refers to the angle between the landing acceleration and the local normal at (x_i, y_j) as depicted in Fig. 6.

Usually, the vehicle can tolerate a certain degree of collision caused by vertical landing velocity [8] but still the collision should be avoided in case of damaging the legs and onboard equipment. Besides, if the vehicle lands on the surface with a certain horizontal velocity and an improper attitude, a tipping over or rolling motion is likely to happen. In asteroid landing missions, these factors are particularly non-ignorable since large velocity and bad landing angle may cause the lander to

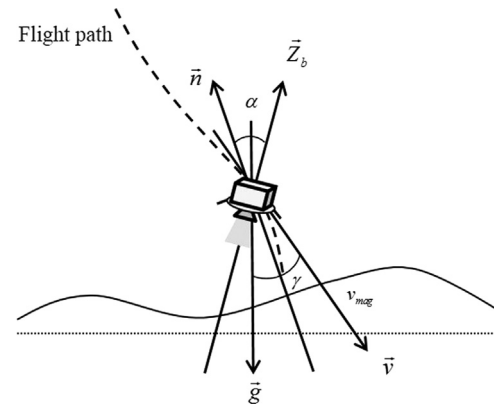


Fig. 6. Touchdown angles illustration.

rebound off the planet and drift away into space [25].

As the descent phase commences, the computer onboard estimates the descent velocity, flight path angles and attitude angles at a certain distance above different landing locations via numerical integration of motion equation and local terrain condition. Landing sites that have small landing velocities and attitude angles are favorable in the subsequent selection process. Although the remaining velocity and the inclined angle of the vehicle can be further decreased by thrusters and attitude control system, or a modified descent architecture, we assume the extra effort is the less the better.

Given a 5% execution error [26] and a 7 m/s steady wind disturbance [27], a simple simulation is conducted using the polynomial guidance law and the terrain model mentioned above. The execution error is added on the nominal acceleration while the wind disturbance impacts directly on the descent velocity. The landing velocity magnitude v_f , the flight path angle γ , and the attitude angle α at 5 m above ground level (AGL) are calculated and illustrated in Figs. 7–9.

2.4. Landing site selection problem

Combining the three factors mentioned above, the optimal landing site is supposed to be a place of large enough safe radius that satisfies fuel consumption and touchdown performance constraints at the same time. From the perspective of landing safety, the landing site selection problem can be described as an optimization problem in the following form

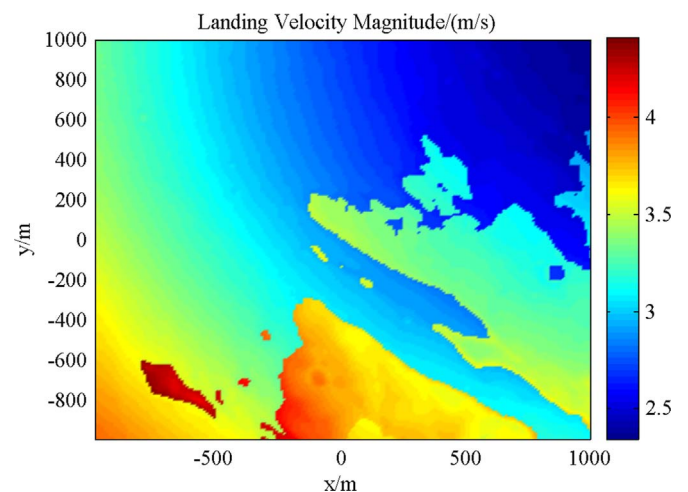


Fig. 7. Landing velocity magnitude variation.

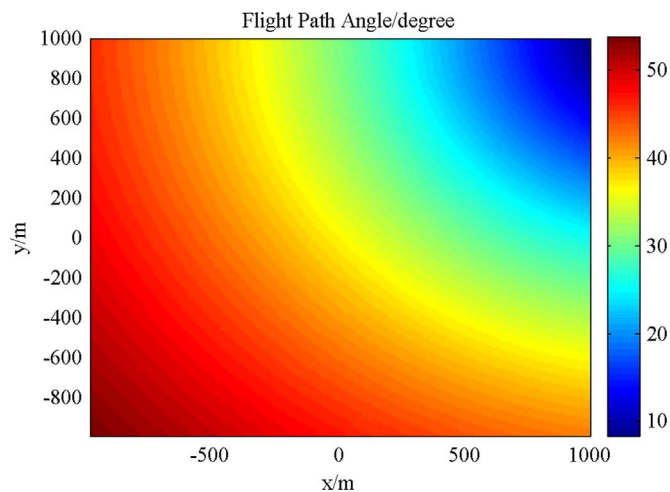


Fig. 8. Flight path angle variation.

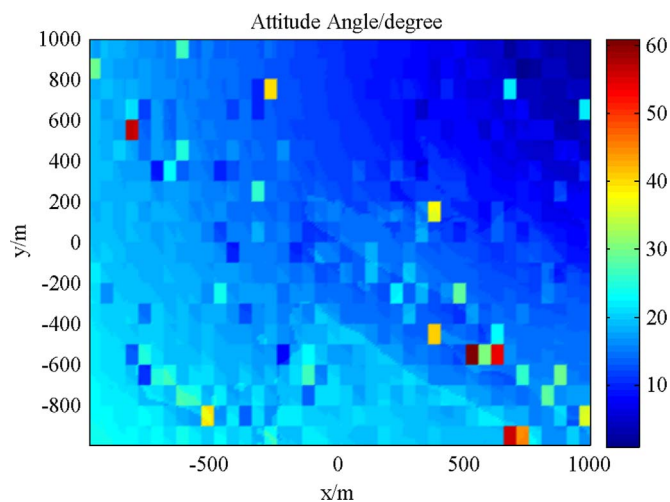


Fig. 9. Landing attitude angle variation.

$$\begin{aligned}
 & \min -R_{ij} \\
 & s. t. \quad \text{PMF}_{ij} \leq \overline{\text{PMF}} \\
 & \quad \quad \|v_f\|_{ij} \leq \overline{v_f} \\
 & \quad \quad \gamma_{ij} \leq \overline{\gamma}, \quad \alpha_{ij} \leq \overline{\alpha}
 \end{aligned} \tag{12}$$

where $\overline{\text{PMF}}$, $\overline{v_f}$, $\overline{\gamma}$, $\overline{\alpha}$ refer to the engineering constraints of the mission. The optimal solution of the problem (x_i^*, y_j^*) is deemed to be the final landing site. Although other constraints that should be met at the same time like dynamic equations, initial conditions, etc., are not shown in Eq. (12), they will be considered when computing the values of PMF, $\|v_f\|$, γ , α at different landing sites.

In order to solve this problem, the mathematical expressions of terrain safety, fuel consumption and touchdown performance with regard to the terminal position vector (x_i, y_j) should be specified first. This process, however, complicates the original problem and increases computation effort. When deducing the safe radius expression, for example, a three-dimensional surface fitting needs to be applied to obtain the continuous terrain relief function. To achieve good fitness, the order of the surface equation should be high, which may lead to a long and sophisticated expression. Besides the complexity of online surface fitting realization, the terrain characteristics like rocks and slopes may be lost in the fitting process and this will severely impact the hazard detection result. The expressions of fuel consumption and touchdown performance are even harder to derive since they are determined synthetically by the adopted guidance law, the terrain condition in the vicinity of the landing site, and the disturbance during descent.

The solving process is also a challenge for optimization methods. On one hand, the convexity of the original problem is not guaranteed and the transformation from the non-convex to the convex is of skill. On the other hand, to avoid ending up with a local optimum, a global optimization method is required, which, however, is usually bounded by its convergence condition and searching speed. Besides, global optimization methods may bring new problems for online implementation due to the memory and operation limits of onboard computers.

In short, the problem cannot be effectively solved using traditional optimization methods owing to its discrete and complex features. Thus, we transform the optimization problem into a one-dimensional search of a synthetic index which covers all the necessary factors in landing site selection and the detailed process is given in the next section.

3. Optimal landing site selection

3.1. Safety index

In this paper, a safety index is proposed as a solution of the landing site selection optimization problem by integrating the optimization index and the constraints into one mathematical expression. First, we need to unify the forms of the variables in the safety index. The typical parameters appeared in the optimization problem can be marked as

$$f_{ij}^t = R_{ij} \tag{13}$$

$$f_{ij}^f = \text{PMF}_{ij} \tag{14}$$

$$\begin{cases} f_{ij}^{p1} = \|v_f\|_{ij} \\ f_{ij}^{p2} = \gamma_{ij} \\ f_{ij}^{p3} = \alpha_{ij} \end{cases} \tag{15}$$

where f_{ij}^t , f_{ij}^f , f_{ij}^p stand for terrain safety function, fuel consumption function and touchdown performance function at (x_i, y_j) respectively. Then the safety index of the point (x_i, y_j) can be written as the sum of the functions

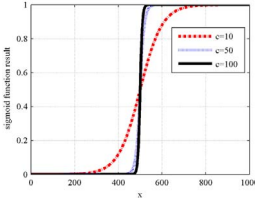
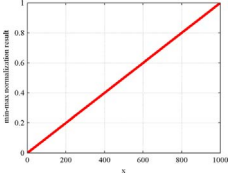
$$SI_{ij} = \tau_1 g_1(f_{ij}^t) + \tau_2 g_2(f_{ij}^f) + \tau_3 g_3(f_{ij}^p) \tag{16}$$

where τ_1 , τ_2 , τ_3 are the weighting coefficients determined by the importance of each factor in the mission. Without loss of generality, we assume the smaller the index gets, the safer the landing area is. Thus, the final landing site is deemed to be at the minimum of the index.

To eliminate the effect of data dimension and quantity, mapping functions are applied to transform the values of every part of the index to the interval between 0 and 1. Two common mapping functions are listed and compared in Table 1. The modified sigmoid function introduces a threshold x_{ij} in the function and generates an s-shape curve as the variable changes. When the variable is smaller than the threshold, the function increases to 1, and decreases to 0 when the variable is larger than the threshold. However, when the variable is close to the threshold, the value of the function changes significantly and the changing rate is controlled by the constant c . In the optimization problem, factors that have explicit engineering constraints like fuel consumption, landing velocity magnitude, flight path angle and landing attitude angle are suitable for using the sigmoid mapping function so that their thresholds can be added into the assessment process. Determined by the data's maximum and minimum value, the min-max normalization is easy to compute and reserves the distribution characteristics of the original data. In the landing site selection process, the safe radius of each potential landing site is the larger the better and does not have a strict lower bound. Thus, the terrain safety component in the safety index is normalized via the min-max normalization method.

Based on the mission requirements and the form of the optimization problem, the safety index is formulated as

Table 1
Mapping function comparison.

	Modified sigmoid function	Min-max normalization
Mapping function	$g(x) = \frac{1}{1 + e^{c(1-x/d)}}$	$g(x) = \frac{x - x_{\min}}{x_{\max} - x_{\min}}$
Value	(0,1)	[0,1]
Feature	Compared with a threshold, near-binary result	Simple and easy, distribution reserved
Illustration		

$$\begin{aligned}
 SI_{ij} = & \tau_1 \left(1 - \frac{f_{ij}^f - f_{\min}^f}{f_{\max}^f - f_{\min}^f} \right) + \tau_2 \frac{1}{1 + e^{c_f(1-f_{ij}^f/f_{\bar{f}})}} + \tau_3 \frac{1}{1 + e^{c_{p1}(1-f_{ij}^{p1}/\bar{f}_{p1})}} \\
 & + \tau_4 \frac{1}{1 + e^{c_{p2}(1-f_{ij}^{p2}/\bar{f}_{p2})}} + \tau_5 \frac{1}{1 + e^{c_{p3}(1-f_{ij}^{p3}/\bar{f}_{p3})}}
 \end{aligned} \tag{17}$$

where \bar{f}_f , \bar{f}_{p1} , \bar{f}_{p2} , \bar{f}_{p3} are the upper thresholds of fuel consumption, landing velocity magnitude, flight path angle and attitude angle respectively, and the weighting coefficient τ_i represents the importance of each factor. The variation range of the safety index is between 0 and 5.

The proposed index can be regarded as a generalized assessment criterion of landing area from the safety point of view and also a landing site selection method. By covering necessary factors in the selection process, the chosen landing site not only is free of hazards, but also guarantees a good landing performance with less fuel consumption.

3.2. Landing site selection process

If the safety indices of all the pixels within the map are calculated, a large amount of computation is required and it usually takes a long time before getting the expected result, which is inappropriate for online implementation. When searching for the final landing site for the mission, the points of large safe radiuses are more appealing as they ensure a relatively large piece of area around them is hazard-free. Usually, if point A has a satisfactory safe radius, the points in its vicinity will also end up with a good result, according to the definition of safe radius. Hence, the fore-mentioned appealing points are very likely to be highly-gathered in several decentralized places in the map. In order to efficiently locate a proper place for landing, the selection scope is reduced by only calculating the safety indices of the points whose safe radiuses are beyond a certain level. The threshold of the safe radius \underline{R} can be determined by, for example, the lander size, the estimated navigation error and/or the average safe radius of the whole map. In this way, only a few points (assume the sample size is M) are under consideration in the subsequent assessment process, which cuts down the computation effort significantly. Since the optimal landing site is a place of large safe radius, little fuel consumption and good touchdown performance (the values of the parameters are small), and the sample process only sifts out the points of small safe radius, the optimal solution is reserved in the M points theoretically. However, it is noted that the sample size depends on the threshold only. If the value of \underline{R} is too large, the sample size will be small. On this occasion, the optimal solution may be as well sifted in extreme conditions where the fuel consumption and touchdown performance are unsatisfactory at all the sample points of large safe radius. On the other hand, if the value of

\underline{R} is too small, the sample size will be large and the computation cut-down effect will be poor. Hence, the safe radius threshold is set after synthetically considering mission requirements, sample size and computation effort.

The safety index-based landing site selection process can be expressed as:

- 1) Evaluate the terrain safety of the whole area and compute the safe radius R_{ij} of each pixel using the algorithm in Section 2.
- 2) Compare the result with the given safe radius threshold \underline{R} . If $R_{ij} < \underline{R}$, set the safety index of the point SI_{ij} as 5 which is the maximum value the safety index can get. On the contrary, if $R_{ij} \geq \underline{R}$, the coordinate of the point (x_i, y_j) and its elevation z_{ij} are saved in the matrix P for further analysis.
- 3) Calculate the safety indices of the M sifted points in step 2) using Eq. (17) and save them in the fourth column of the P matrix. In this way, each row of the matrix contains the 3D coordinate of every sifted point and the corresponding safety index value in the following form.

$$P = \begin{bmatrix} x_1 & y_1 & z_1 & SI_1 \\ x_2 & y_2 & z_2 & SI_2 \\ \vdots & \vdots & \vdots & \vdots \\ x_M & y_M & z_M & SI_M \end{bmatrix} \tag{18}$$

- 4) Conduct a traversal search using the classic bubble sort to locate the minimum safety index whose location is set as the final landing site. The bubble sort is used in the P matrix from the top to the bottom. To begin with, the fourth elements in the first two rows are compared. If SI_1 is larger than SI_2 , go on and compare the fourth elements in the second and the third rows. Otherwise, switch all the elements in the first row with those of the second row before comparing the safety indices in the second and the third rows. The process continues until all the elements in the fourth column are compared. In the end, the minimum safety index, together with its coordinates, are switched to the last row of P and output to the subsequent guidance and control system which diverts the vehicle from its current position to the new destination.

Note that by implementing the bubble sort, the minimum value of the safety index and its corresponding coordinate are rapidly found after only one iteration. If two or more landing sites are needed as backup solutions, the number of iteration increases accordingly by repeating the same process mentioned in step 4).

3.3. Implementation in planetary missions

The safety index-based landing site selection method is flexible and can be adjusted according to different planetary exploration missions. For example, if more factors are considered in the landing site selection problem in Eq. (12), similar transformation can be carried out to add the new elements into the safety index expression. Besides, the values of the weighting coefficients in the index are determined by the priority concerns of the mission. When implementing the method in practice, there are some differences between major planet missions and asteroid/comet missions.

Compared with other objects in the solar system, asteroids and comets are small in size and irregular in shape, resulting in a weak and changing gravitational pull [28]. Landing on an asteroid or comet usually takes a longer time and the descent speed is relatively small. Due to weak gravity, large landing velocity and improper landing attitude may cause the vehicle to bounce off the surface or even escape into space. Besides, environmental perturbations and navigation/execution errors are more obvious in the descent process, which sets higher requirements on dynamic modeling accuracy and GNC system robustness. Thus, when selecting the landing site and designing the safety index for asteroid/comet exploration missions, these factors

should be considered prior and the relevant items can be added in the touchdown performance component with an increment of the weights in the safety index.

On the other hand, as a typical major planet of great scientific interest, Mars is bigger in size and has a relatively strong gravitational field. Its surface is distributed with irregular rocks and craters. These hazards may threaten landing safety and cannot be precisely detected in advance until the spacecraft is close enough to the surface. Besides, the descending speed is very fast and the whole landing process takes only several minutes. In Mars exploration missions, terrain detection begins after the heatshield is separated from the vehicle during parachute descent phase and leaves only less than two minutes to go. In such cases, the vehicle has to determine the safe region and select the best landing site via the onboard computer within a short time. Hence, compared with asteroid and comet missions, terrain safety and computation efficiency are the main concerns in major planets exploration.

4. Simulation

4.1. MSL-based simulation model

Without loss of generality, the Mars landing process is used to verify the effectiveness of the safety index method. A 400 m × 400 m terrain model of the MSL landing site is built based on the DEM data acquired by HiRISE at the resolution of 0.25 m/pixel in Fig. 10. By implementing the proposed safety index in the model, we show the capability of the method in landing site selection. Simulation parameters are given based on the MSL mission [24] and are listed in Table 2.

The dynamics of powered descent phase can be expressed as [29]

$$\begin{aligned} \dot{x} &= u & \dot{y} &= v & \dot{z} &= w \\ \dot{u} &= \Gamma \sin \theta \cos \psi \\ \dot{v} &= \Gamma \sin \psi \\ \dot{w} &= -g + \Gamma \cos \theta \cos \psi \\ \Gamma &= \frac{T}{m} \end{aligned} \quad (19)$$

where $(x, y, z)^T$ are the position vectors and $(u, v, w)^T$ are the velocity vectors, Γ is the magnitude of the specific thrust, and the angles θ and ψ illustrated in Fig. 11 serve as the thrust direction and attitude coordinates.

The powered descent guidance used in the MSL lander is a derivative of the Apollo lunar descent guidance [30]. Assume the

Table 2
Powered descent parameters in the MSL mission.

Parameter	Value
Maximum engine thrust, N	3100
Engine I_{sp} , s	225
Earth gravitational acceleration, m/s ²	9.807
Mars gravitational acceleration, m/s ²	3.7114
Initial mass, kg	1905
Fuel mass, kg	400
Initial position, m	$[-500 \ -800 \ 1620]^T$
Initial velocity, m/s	$[20 \ 20 \ -125]^T$
Slope	2–5 m length scale: $\leq 15^\circ$
Roughness	≤ 0.5 m

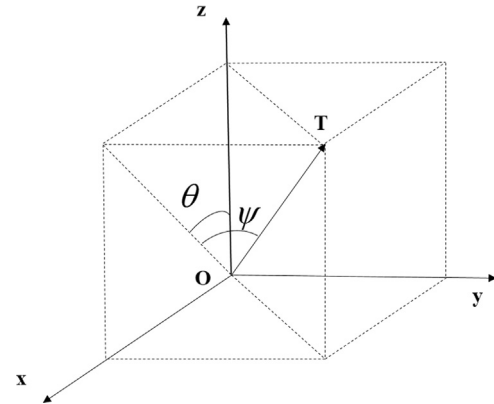


Fig. 11. Thrust vector and its components in three axes under the inertial coordinate system.

acceleration in each direction is a quadratic polynomial of time in the following form

$$a(t) = C_0 + C_1 t + C_2 t^2 \quad (20)$$

The velocity and position variation with time can be then obtained by integration. Given the initial and terminal conditions

$$\begin{cases} \mathbf{r}(0) = \mathbf{r}_0, & \mathbf{v}(0) = \mathbf{v}_0 \\ \mathbf{r}(t_f) = \mathbf{r}_f, & \mathbf{v}(t_f) = \mathbf{v}_f, & \mathbf{a}(t_f) = \mathbf{a}_f \end{cases} \quad (21)$$

the coefficients in the acceleration expression are solved as [22]

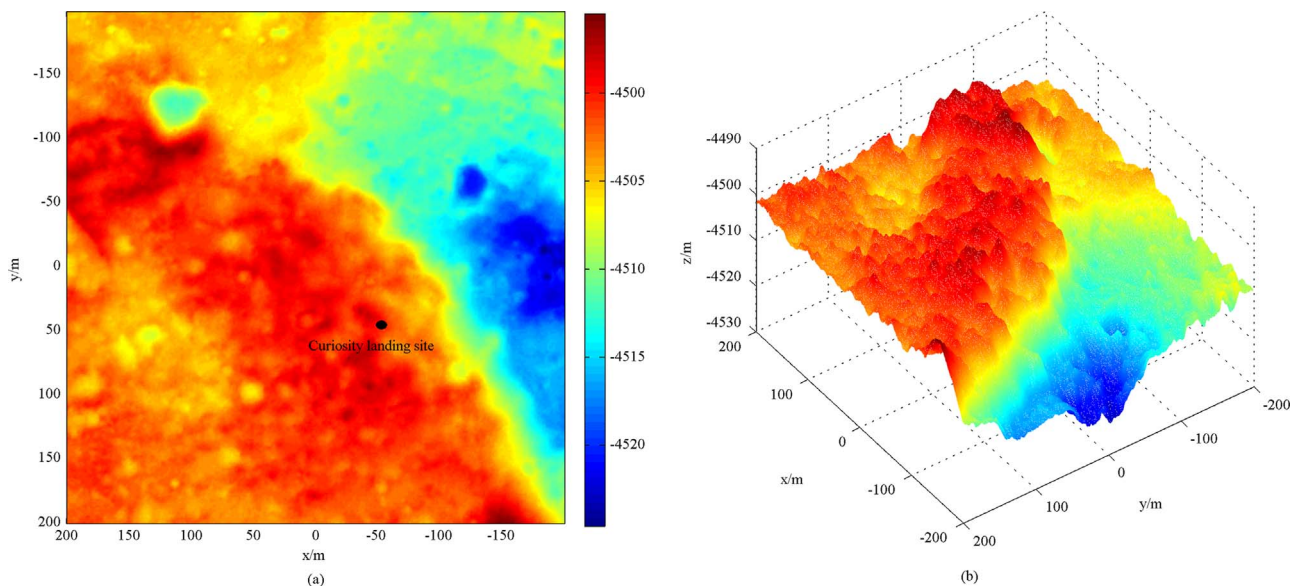


Fig. 10. The 2D and 3D topography of Curiosity's landing site.

$$\begin{aligned}
 C_0 &= a_f - \frac{6}{t_{go}}(v_f + v_0) + \frac{12}{t_{go}^2}(r_f - r_0) \\
 C_1 &= -\frac{6}{t_{go}}a_f + \frac{6}{t_{go}^2}(5v_f + 3v_0) - \frac{48}{t_{go}^3}(r_f - r_0) \\
 C_2 &= \frac{6}{t_{go}^2}a_f - \frac{12}{t_{go}^3}(2v_f + v_0) + \frac{36}{t_{go}^4}(r_f - r_0)
 \end{aligned} \tag{22}$$

where t_{go} refers to the time to go before touch-down. To simplify analysis, the direction of the thrust vector is considered aligned with the vertical axis of the lander.

4.2. Landing site selection using safety index

Before assessing the landing area using the proposed safety index method, every item in the index needs to be specified first.

Slopes and roughness of the assessment area are computed based on the DEM data. A grid map is generated with a resolution of 1 m/pixel and the pixels are classified into the safe and the hazardous after comparison with the slope and roughness constraints. The safe radius map is obtained using the ergodic search algorithm and the result is shown in Fig. 12. It is observed that the variation range of the safe radius is between 0 m and 27 m. Thus, the parameters f_{min}^t and f_{max}^t in the terrain safety function are set as 0 and 27 respectively. Considering the safe radius range and the size of the lander, the landing site selection scope is reduced by setting the safe radius threshold R as 10 m. The sift result is illustrated in Fig. 13. The white area (set as 1) refers to the points whose safe radiuses are larger than the threshold and are deemed to be the landing site candidates, while the black area (set as 0) refers to the points with smaller safe radiuses whose safety indices are directly set as the maximum value 5. In this example, the landing site selection scope is efficiently reduced to 6% of the original area.

According to the system parameters in Table 2, the threshold in the fuel consumption function is calculated by

$$\bar{f}_f = PMF_{max} = \frac{m_{fuel}}{m_0} = 0.2100 \tag{23}$$

In the simulation, all the weights in the safety index are set as 1 as every factor is deemed to be equally important in the paper. In the powered descent phase, the landing performance of the vehicle is influenced by both internal and external disturbances. In this simulation, a 5% execution error and a 7 m/s steady wind disturbance are applied to assess the robustness of the polynomial guidance. The complete index parameter settings are listed in Table 3.

The safety indices of the points in the white area in Fig. 13 are computed then using the specified safety index expression

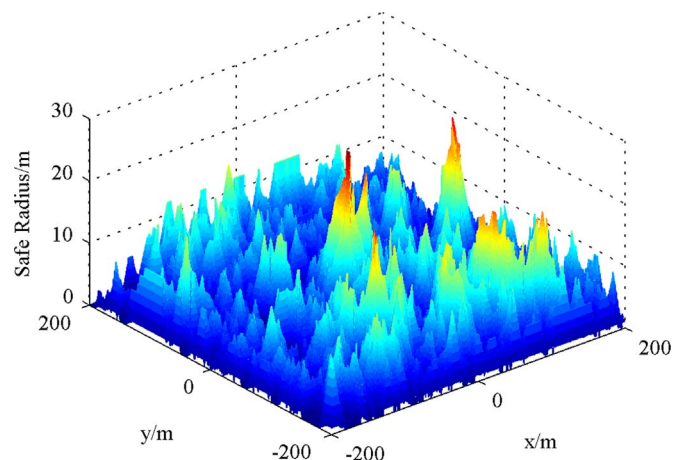


Fig. 12. The safe radius variation.

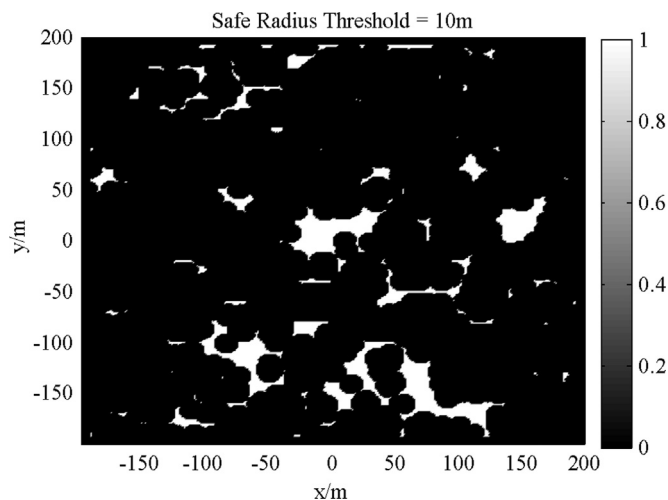


Fig. 13. The selection scope is reduced to the white areas.

Table 3
Parameter settings in the safety index.

Parameter	Value
Safe radius minimum f_{min}^t	0 m
Safe radius maximum f_{max}^t	27 m
Safe radius threshold R	10 m
Fuel consumption threshold \bar{f}_f	0.2100
Velocity magnitude threshold \bar{v}_{p1}	4 m/s
Flight path angle threshold $\bar{\theta}_{p2}$	30°
Attitude angle threshold $\bar{\theta}_{p3}$	30°
$c_f, c_{p1}, c_{p2}, c_{p3}$	50
$\tau_1, \tau_2, \tau_3, \tau_4, \tau_5$	1
Execution error	5%
Wind disturbance on velocity	7 m/s

$$\begin{aligned}
 SI_i &= 1 - \frac{f_i^t}{27} + \frac{1}{1 + e^{50(1-f_i^t/0.2100)}} + \frac{1}{1 + e^{50(1-f_i^{p1}/4)}} + \frac{1}{1 + e^{50(1-f_i^{p2}/30)}} \\
 &+ \frac{1}{1 + e^{50(1-f_i^{p3}/30)}}
 \end{aligned} \tag{24}$$

and the results are shown in Fig. 14.

The point with the smallest safety index value is chosen to be the final landing site of the mission. In this simulation, the point (-12, 3) with a safety index of 1.0792 is selected. Together with the original

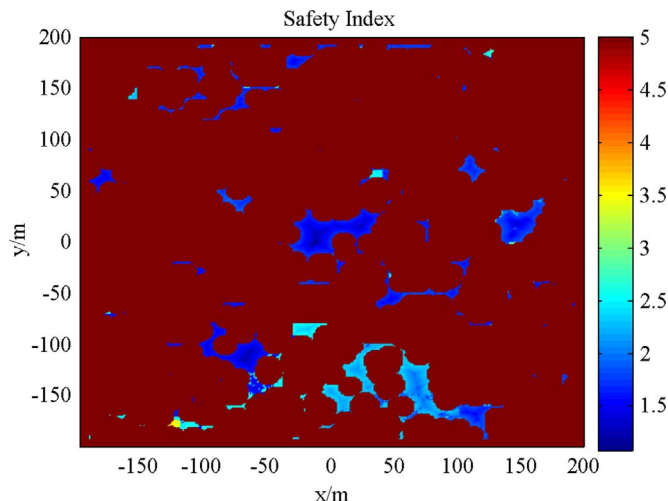


Fig. 14. Safety index computation result.

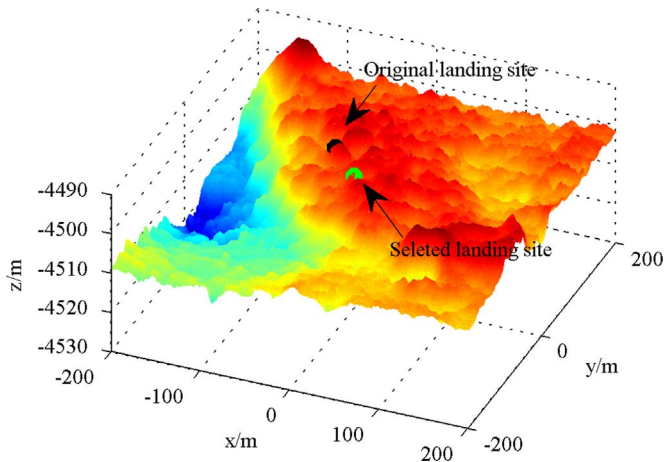


Fig. 15. Location of the selected landing site.

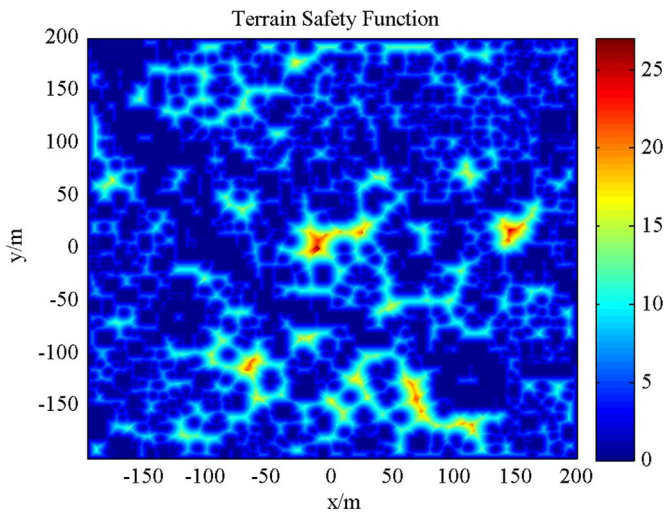


Fig. 16. Variation of the terrain safety function.

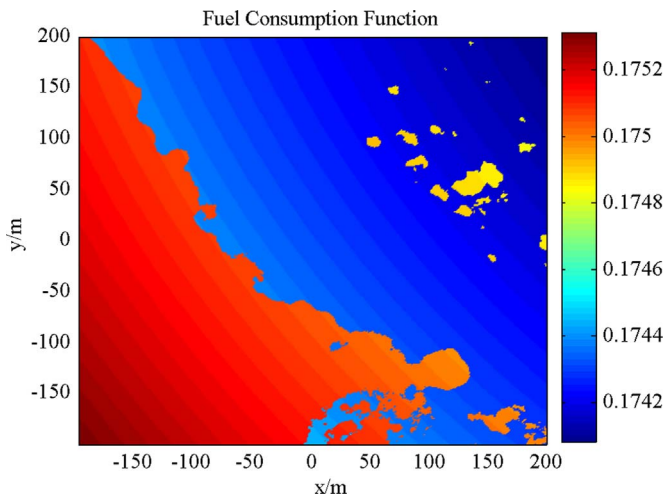


Fig. 17. Variation of the fuel consumption function.

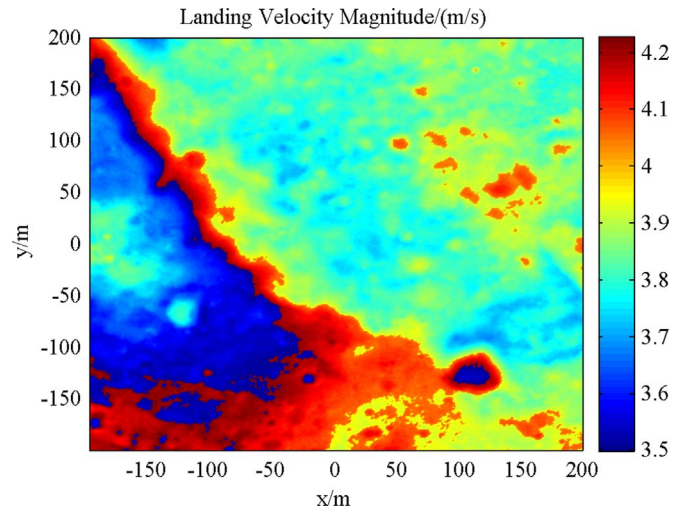


Fig. 18. Variation of the landing velocity magnitude.

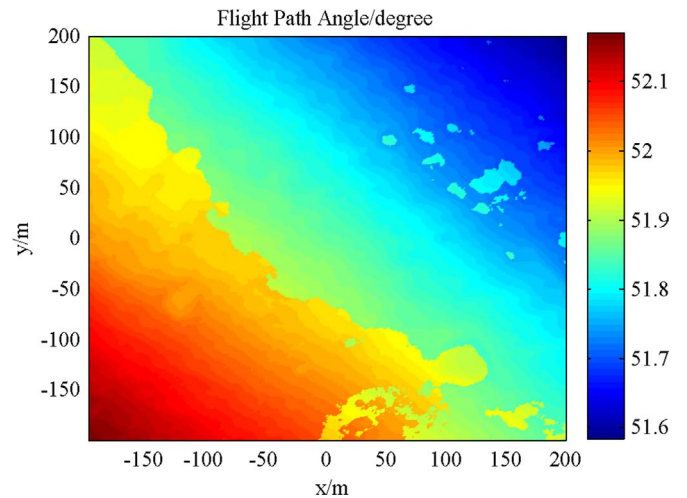


Fig. 19. Variation of the flight path angle.

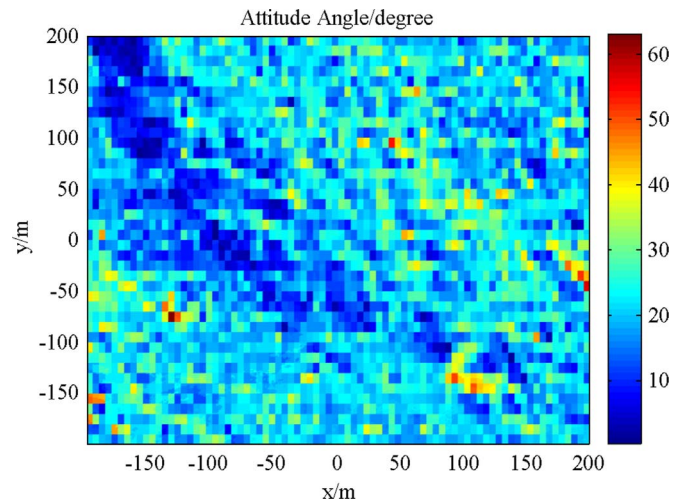


Fig. 20. Variation of the attitude angle.

landing site of the MSL mission, the location of the new landing site is shown in Fig. 15. As can be seen, the safety index-selected landing site is close to the original landing site (about 60 m away) but on a flatter surface. It is further away from the steep edge where elevation changes rapidly and ensures the safety of the mission with a 27 m landing error tolerance.

4.3. Selection result verification

In order to verify the landing site selection result, the safety index value of the whole area is calculated. All the points in the map are assessed using the safety index and it takes a relatively longer time to

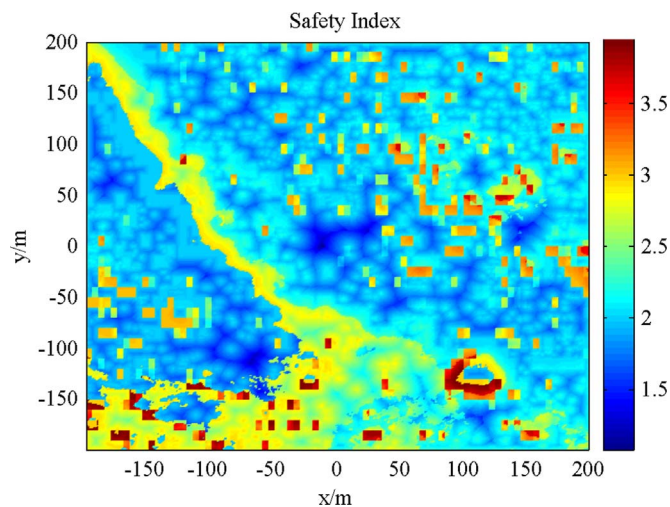


Fig. 21. Safety index computation result.

Table 4
Landing site selection results.

	Landing site location	Safety index value
MSL landing site	(−50, 45, −4499.8)	1.8819
Selected landing site	(−12, 3, −4500.3)	1.0792
Global optimal landing site	(−12, 3, −4500.3)	1.0792

get the overall safety index map due to the large computation effort. The variations of the terrain safety function, fuel consumption function, touchdown performance functions and their sum are shown in Figs. 16–21 respectively.

The safety index value of the whole map is supposed to be between 0 and 5. But the minimum in Fig. 21 is larger than 1. This is mainly because all the flight path angles calculated at 5 m AGL are larger than the given threshold. Compared with Fig. 8, the variation range of the flight path angle in the simulation is relatively small due to the limited size of the assessment area. Even though large flight path angles, which means inclined velocity directions, are not wanted from the perspective of safety, the three components of the velocity at 5 m AGL are small as indicated in Fig. 18. Thus, the remaining landing velocity and the improper attitude can be further adjusted in the last 5 m via onboard equipment. It is also noted that the maximum in Fig. 21 is no bigger than 4, which is the result of no violation of the fuel consumption constraint in the whole assessment area as shown in Fig. 17. The PMF variation range is determined by the guidance law adopted. In this paper, the polynomial guidance shows a good consistency in fuel consumption regardless of the change of landing sites. In future missions, other guidance laws will be implemented during descent and the fuel consumption distribution characteristics may be different.

After a traversal search, the global optimal landing site is then chosen at the minimum of the safety index. The location of the landing site and its corresponding safety index value are compared with the MSL landing site and the previously selected landing site in Table 4. As can be seen, the selected landing site overlaps with the global optimal solution. The result confirms that the optimal landing site is among the safe radius-based reduced scope which only accounts for 6% of the original area. The simulation result proves that the proposed safety index method manages to efficiently select a safe landing site for the mission with only a small amount of computation.

5. Conclusion

In this paper, multiple factors that affect landing safety, including terrain safety, fuel consumption and touchdown performance, are

analyzed and the landing site selection process is converted into an optimization problem. The problem is then solved using the proposed safety index method and the optimal landing site is obtained after a simple one-dimensional search. For better online implementation, the selection scope is further reduced by setting a threshold for the safe radius, which cuts down the computation effort significantly. The method is flexible when applied in different exploration missions. The result of the simulation based on the past successful mission suggests that the safety index method manages to assess the landing area from the given aspects and accomplishes the work of landing site selection efficiently.

For future planetary exploration missions, the safety index can be used as a generalized assessment criterion of the landing area. By covering necessary factors, the index is able to quickly select the best landing site that is far away from the hazards while satisfying the engineering constraints at the same time, which provides practical solutions for online landing site selection problems.

Acknowledgements

This work was supported in part by the following grants: National Basic Research Program of China (973 Program) 2012CB720000, the National Natural Science Foundation of China 61374216, 61304226, and 61304248, the Research Fund for the Doctoral Program of Higher Education of China 20111101110001, and Science and Technology Innovation Team of Beijing Institute of Technology.

References

- [1] S.R. Ploen, H. Seraji, C.E. Kinney, Determination of spacecraft landing footprint for safe planetary landing, *IEEE Trans. Aerosp. Electron. Syst.* 45 (2009) 3–16.
- [2] M.P. Golombek, R.A. Cook, T. Economou, W.M. Folkner, A.F.C. Haldemann, et al., Overview of the Mars pathfinder mission and assessment of landing site predictions, *Science* 278 (1997) 1743–1748.
- [3] R. Fisackerly, A. Pradier, B. Gardini, B. Houdou, C. Philippe, et al., The ESA lunar lander mission, in: *Proceedings of the AIAA Space 2011 Conference & Exposition, AIAA 2011–7217*, Long Beach, CA, 27–29 September, 2011.
- [4] S. Ulamec, J. Biele, A. Blazquez, B. Cozzoni, C. Delmas, et al., Rosetta lander – Philae: landing preparations, *Acta Astronaut.* 107 (2015) 79–86.
- [5] J.M. Hurtado Jr., K. Young, J.E. Bleacher, W.B. Garry, J.W. Rice Jr., Field geologic observation and sample collection strategies for planetary surface exploration: Insights from the 2010 Desert RATS geologist crewmembers, *Acta Astronaut.* 90 (2013) 344–355.
- [6] A.L. Strahan, A.E. Johnson, Terrain hazard detection and avoidance during the descent and landing phase of the Altair mission, in: *Proceedings of the AIAA Guidance, Navigation, and Control Conference, AIAA 2010–7722*, Toronto, Ontario Canada, 2–5 August, 2010.
- [7] Y. Guo, M. Hawkins, B. Wie, Waypoint-optimized zero-effort-miss/zero-effort-velocity feedback guidance for Mars landing, *J. Guid. Control Dyn.* 36 (2013) 799–809.
- [8] D.W. Dunham, R.W. Farquhar, J.V. McAdams, M. Holdridge, R. Nelson, et al., Implementation of the first asteroid landing, *Icarus* 159 (2002) 433–438.
- [9] X. Jiang, S. Li, T. Tao, Innovative hazard detection and avoidance strategy for autonomous safe planetary landing, *Acta Astronaut.* 126 (2016) 66–76.
- [10] B.E. Cohanin, B.K. Collins, Landing point designation algorithm for lunar landing, *J. Spacecr. Rockets* 46 (2009) 858–864.
- [11] J. Kawaguchi, Hayabusa, summary of guidance, navigation and control achievement in its proximity phase, in: *Proceedings of the AIAA/AAS Astrodynamics Specialist Conference and Exhibit, AIAA 2006–6533*, Keystone, CO, 21–24 August, 2006.
- [12] A.A. Wolf, B. Acikmese, Y. Cheng, J. Casoliva, J.M. Carson, et al., Toward improved landing precision on Mars, in: *Proceedings of the IEEE Aerospace Conference, Paper 1209*, Bigsky, MT, 5–12 March, 2011.
- [13] A.G. Ge, P. Cui, Online landing site selection considering maneuverability constraint during Mars powered descent phase, in: *Proceedings of the AIAA Guidance, Navigation, and Control Conference, AIAA 2016–1134*, San Diego, CA, 4–8 January, 2016.
- [14] P. Rogata, E.D. Sotto, F. Câmara, et al., Design and performance assessment of hazard avoidance techniques for vision-based landing, *Acta Astronaut.* 61 (2007) 63–77.
- [15] A. Johnson, A.R. Klumpp, J.B. Collier, A.A. Wolf, Lidar-based hazard avoidance for safe landing on Mars, *J. Guid. Control Dyn.* 25 (2002) 1091–1099.
- [16] S. Li, X. Jiang, T. Tao, Guidance summary and assessment of the Chang'e-3 powered descent and landing, *J. Spacecr. Rockets* 53 (2016) 258–277.
- [17] N. Serrano, A bayesian framework for landing site selection during autonomous spacecraft descent, in: *Proceedings of the Intelligent Robots and Systems, 2006 IEEE/RSJ International Conference*, Beijing, China, 9–15 October, 2006.
- [18] R.D. Braun, R.M. Manning, Mars exploration entry, descent and landing chal-

- lenges, *J. Spacecr. Rockets* 44 (2007) 310–323.
- [19] A.Howard, H.Seraji, A fuzzy rule-based safety index for landing site risk assessment, in: *Automation Congress, 2002 Proceedings of the 5th Biannual World*, 14, 2002, pp. 579–584.
- [20] W. Wu, D. Wang, X. Huang, et al., Autonomous hazard detection and avoidance guidance method for soft lunar landing, *Sci. Sin. Inf.* 45 (2015) 1046–1059.
- [21] A.B.Acikmese, S.R.Ploen, A powered descent guidance algorithm for Mars pinpoint landing. *AIAA paper*, pp. 2005–6288, 2005.
- [22] B.A. Steinfeldt, M.J. Grant, D.A. Matz, R.D. Braun, G.H. Barton, Guidance, navigation, and control system performance trades for Mars pinpoint landing, *J. Spacecr. Rockets* 47 (2010) 188–198.
- [23] L. Witte, et al., Rosetta lander Philae – landing performance and touchdown safety assessment, *Acta Astronaut.* 125 (2016) 149–160.
- [24] R.Prakash, P.D.Burkhart, A.Chen, K.A.Comeaux, C.S.Guernsey, et al., Mars science laboratory entry, descent, and landing system overview, in: *Proceedings of the IEEE Aerospace Conference*, Paper 1531, Bigsky, MT, 1–8 March, 2008.
- [25] E. Hand, Philae probe makes bumpy touchdown on a comet, *Science* 346 (2014) 900–901.
- [26] S.A. Striepe, D.W. Way, A.M. Dwyer, J. Balaram, Mars science laboratory simulations for entry, descent, and landing, *J. Spacecr. Rockets* 43 (2006) 311–323.
- [27] R.D. Lorenz, Martian surface wind speeds described by the Weibull distribution, *J. Spacecr. Rockets* 33 (1996) 754–756.
- [28] R. Furfaro, D. Cersosimo, D.R. Wibben, Asteroid precision landing via multiple sliding surfaces guidance techniques, *J. Guid. Control Dyn.* 36 (2013) 1075–1092.
- [29] U. Topcu, J. Casoliva, K.D. Mease, Minimum-fuel powered descent for Mars pinpoint landing, *J. Spacecr. Rockets* 44 (2007) 324–331.
- [30] E.C. Wong, G. Singh, J.P. Masciarelli, Autonomous guidance and control design for hazard avoidance and safe landing on Mars, *J. Spacecr. Rockets* 43 (2006) 378–384.